

The First Day in the Life of a Magnetar: Evolution of the Inclination Angle, Magnetic Dipole Moment and Braking Index of Millisecond Magnetars During Gamma-Ray Burst Afterglows

SİNEM ŞAŞMAZ MUŞ,¹ SERCAN ÇIKINTOĞLU,¹ UĞUR AYGÜN,¹ İ. CEYHUN ANDAÇ,¹ AND K. YAVUZ EKİŞİ¹

¹*İstanbul Technical University
 Faculty of Science and Letters,
 Physics Engineering Department,
 34469, İstanbul, Turkey*

(Received; Revised; Accepted)

ABSTRACT

The afterglow light curves of some gamma-ray bursts (GRBs) show a shallow decay (plateau) phase implying continuous injection of energy. The source of this energy is very commonly assumed to be the spin-down power of a nascent millisecond magnetar. The magnetic dipole radiation torque is considered to be the mechanism causing the spin-down of the neutron star. This torque has a component working for the alignment of the angle between rotation and magnetic axis, i.e. inclination angle. Here, we demonstrate the evolution of the inclination angle and magnetic dipole moment of nascent magnetars associated with GRBs. We constrain the initial inclination angle, magnetic dipole moment and rotation period of seven magnetars by modelling the seven long-GRB afterglow light curves. We find that, in its first day, the inclination angle of a magnetar decreases rapidly. The rapid alignment of the magnetic and rotation axis may address the lack of persistent radio emission from mature magnetars. We also find that in three cases the magnetic dipole moments of magnetars decrease exponentially to a value a few times smaller than the initial value. The braking index of nascent magnetars, as a result of the alignment and magnetic dipole moment decline, is variable during the afterglow phase and always greater than three.

Keywords: gamma-ray burst: general stars: magnetars

1. INTRODUCTION

The plateau phase in the afterglow emission of GRBs are suggested to be associated with magnetars (Usov 1992; Duncan & Thompson 1992; Kluźniak & Ruderman 1998; Dai & Lu 1998a,b; Zhang & Mészáros 2001; Bucciantini et al. 2008; Metzger et al. 2011) and, therefore frequently modelled by employing the spin-down power of a magnetar (Fan & Xu 2006; Troja et al. 2007; Dall'Osso et al. 2011; Rowlinson et al. 2010, 2013; Gompertz et al. 2013; Fan et al. 2013; Lü & Zhang 2014; Rowlinson et al. 2014; Rea et al. 2015; Lü et al. 2017; Gompertz & Fruchter 2017; Lasky et al. 2017; Knust et al. 2017; Gompertz & Fruchter 2017; Li et al. 2018; Stratta et al. 2018; Lü et al. 2019)

The radiation emitted by a rotating neutron star has long been considered to be due to its magnetic dipole moment and studied in the framework of the magnetic dipole braking model (Gold 1968; Pacini 1968). For a neutron star rotating in vacuum this model predicts a spin-down relation of the form $\dot{\Omega} = -K\Omega^3$ where Ω is the angular velocity of the star, $K \equiv 2(\mu \sin \alpha)^2/(3Ic^3)$, c is the speed of light, μ is the magnetic dipole moment of the star, I is the moment of inertia and α is the inclination angle. From this one can solve the spin-down luminosity, $L_{sd} = -I\Omega\dot{\Omega}$, as $L_{sd} = L_0(1+t/t_0)^{-2}$ where $L_0 = IK\Omega_0^4$ and $t_0 = (2K\Omega_0^2)^{-1}$. This leads to $L_{sd} \propto t^{-2}$ at late time. If the second derivative of the angular velocity ($\ddot{\Omega}$) is measured, the braking index $n \equiv \ddot{\Omega}\Omega/\dot{\Omega}^2$ can be determined. The value of the braking index is used for the assessment of the pulsar spin-down mechanisms and models. Magnetic dipole braking model predicts a constant braking index of $n = 3$. The braking indices of conventional pulsars measured to date (Lyne

et al. 1993, 1996; Livingstone et al. 2007; Espinoza et al. 2011; Livingstone & Kaspi 2011; Roy et al. 2012; Archibald et al. 2015; Ferdman et al. 2015; Antonopoulou et al. 2015) are less than three except for PSR J1640–4631 (Archibald et al. 2016).

Recently, (Lasky et al. 2017) (see also Lü et al. (2019)) have invoked the somewhat more general spin-down relation $\dot{\Omega} \propto -\Omega^n$ for modelling the spin-down of putative magnetars in two *short* GRBs. This model involves the assumption that the braking index is constant and has the solution $L_{\text{sd}} = L_0(1+t/t_0)^{-(n+1)/(n-1)}$. From the fits to the light curves of two *short* GRBs, GRB 130603B and GRB 140903A (Lasky et al. 2017), found the value of the braking indices of the putative magnetars as $n = 2.9 \pm 0.1$ and $n = 2.6 \pm 0.1$, consistent with the measured braking indices of conventional pulsars. For ordinary pulsars with ages of $10^3 - 10^4$ yr the assumption of constant braking index may be reasonable for an episode of 10 days. The light curves of GRB afterglow, on the other hand, from the first second to 10 days, amount to more than 5 decades of data and assuming a constant braking index is not warranted for these cases.

Moreover, the alignment of the inclination angle due to the magnetic dipole torque acting on a neutron star is expected as the system will evolve in a way to reduce the spin-down losses (Philippov et al. 2014), but is usually neglected for ordinary pulsars on the grounds that its progress would be slowed-down, for non-spherical pulsars, by dissipation due to the presence of a solid crust (Goldreich 1970). It is not possible to justify the neglect of the alignment component for nascent magnetars taking role in GRBs as their crust may not have solidified yet as also suggested by Lander & Jones (2018). Xu & Huang (2015) studied the effect of rapid linear change in inclination angle on the light curves of GRB afterglows.

In this work we model the X-ray afterglow light curves of selected GRBs (§2.3) with the spin-down power of a nascent neutron star: $L_X = \eta L_{\text{sd}}$ where η is an efficiency factor for conversion of spin-down power to X-ray luminosity. We assume the star to be spinning-down in the presence of a corotating plasma, under the action of the alignment torque coupled with the spin-down torque (§2.1). When necessary we allowed also for the exponential evolution of the magnetic dipole moment, either growth or decay. We inferred the period, inclination angle, magnetic dipole moment of the star at the start of the plateau phase, evolutionary time scale of the magnetic dipole moment and its relaxed value by following a Bayesian framework (§2.2) and calculated the braking indices of nascent magnetars. In order to sample from posterior probability distributions we used an affine-invariant Markov Chain Monte-Carlo Ensemble sampler, `emcee` (Foreman-Mackey et al. 2013) (§2.2).

2. METHOD

2.1. Model equations

The spin-down (Spitkovsky 2006) and alignment (Philippov et al. 2014) torques in the presence of a corotating plasma (Goldreich & Julian 1969) are

$$I \frac{d\Omega}{dt} = -\frac{\mu^2 \Omega^3}{c^3} (1 + \sin^2 \alpha) \quad (1)$$

$$I \frac{d\alpha}{dt} = -\frac{\mu^2 \Omega^2}{c^3} \sin \alpha \cos \alpha. \quad (2)$$

The alignment in the presence of the corotating plasma is slower compared to the vacuum case (Philippov et al. 2014). In the plasma-filled magnetosphere model the braking index is given as (Arzamasskiy et al. 2015; Ekşioğlu et al. 2016):

$$n = 3 + 2 \left(\frac{\sin \alpha \cos \alpha}{1 + \sin^2 \alpha} \right)^2 \quad (3)$$

The magnetic dipole moment of nascent magnetars could be changing in the time-frame of our analysis either because the magnetic field (Duncan & Thompson 1992; Akiyama et al. 2003; Cheng & Yu 2014) or the radius (Burrows & Lattimer 1986) of a millisecond nascent magnetar could change. To simplify matters we assume that this initial transient stage is described by an exponential relaxation

$$\mu = \mu_\infty + (\mu_0 - \mu_\infty) \exp(-t/t_m) \quad (4)$$

where t_m is the evolutionary time-scale of the magnetic dipole moment, μ_0 is the magnetic dipole moment at the start of the plateau phase and μ_∞ is the value the magnetic dipole moment tends to relax; i.e. the magnetic dipole moment

the star will have for an extended life. In case the magnetic dipole moment evolves simultaneously with the inclination angle, the braking index is given as (Eksi 2017)

$$n = 3 + 2 \left(\frac{\sin \alpha \cos \alpha}{1 + \sin^2 \alpha} \right)^2 + 4 \frac{\tau_c}{\tau_\mu} \quad (5)$$

where $\tau_c \equiv -\Omega/2\dot{\Omega}$ and $\tau_\mu \equiv -\mu/\dot{\mu}$. Using Equation (4) we obtain

$$\tau_\mu = \frac{t_m}{\mu_\infty/\mu - 1} \quad (6)$$

and by using Equation (1)

$$\tau_c = \frac{Ic^3}{2\mu^2\Omega^2(1 + \sin^2 \alpha)}. \quad (7)$$

We assume the X-ray luminosity of the afterglow scales with the spin-down luminosity $L_{sd} = -I\Omega\dot{\Omega}$ so that

$$L_X = \eta \frac{\mu^2\Omega^4}{c^3} (1 + \sin^2 \alpha) \quad (8)$$

where η is a constant. This factor not only represents how efficiently the spin-down luminosity is converted into X-rays in the observed band, but also takes care of the beaming hence can be greater than unity.

2.2. Parameter estimation

Our parameter sets are $\{P_0, \sin \alpha_0, \mu_0\}$ for the constant magnetic dipole moment case and $\{P_0, \sin \alpha_0, \mu_0, \mu_\infty, t_m\}$ for the changing magnetic dipole moment case.

The efficiency factor η in Equation (8) is not a parameter that could be determined independent of μ_0 and P_0 . Because of the underlying symmetry of the equations, $P_0 \rightarrow P_0\sqrt{\eta}$ and $\mu_0 \rightarrow \mu_0\sqrt{\eta}$ will result with the same light curve. In the following, we present results obtained for $\eta = 1$. However, using the underlying symmetry above one can easily estimate the P_0 and μ_0 values that would give the same results for a different value of η (see Figure 8).

In order to estimate the nascent magnetar parameters and their credible regions we followed the Bayesian approach. The posterior probability distribution, following Bayes' theorem, is defined as (Sivia & Skilling 2006)

$$\text{prob}(\text{hypothesis}|\text{data}, I) = \frac{\text{prob}(\text{data}|\text{hypothesis}, I) \times \text{prob}(\text{hypothesis}|I)}{\text{prob}(\text{data}|I)} \quad (9)$$

Here, I is the background information which is usually omitted in the representation of the theorem, $\text{prob}(\text{hypothesis} | I)$ is the prior probability which represents our prior knowledge on the parameters of the hypothesis and $\text{prob}(\text{data} | \text{hypothesis}, I)$, i.e. likelihood, probability of obtaining the data given that our hypothesis is true. $\text{prob}(\text{data} | I)$ is the probability of our data which is also called as evidence and can be omitted in the parameter estimation applications since it will behave like a normalization factor (Sivia & Skilling 2006).

Thus, we can write the posterior probability distribution as

$$\text{posterior} \propto \text{likelihood} \times \text{prior}. \quad (10)$$

Here, we used a Gaussian ln-likelihood function¹ such that

$$\ln(\text{likelihood}) = -\frac{1}{2} \left[\sum_{i=1}^N \frac{(y_i - f(\theta_i))^2}{\sigma_{y,i}^2} + \ln(2\pi\sigma_{y,i}^2) \right] \quad (11)$$

and uniform prior probability in specified parameter ranges (see Table 1)

$$\ln(\text{prior}) = \begin{cases} 0, & \text{if } \theta_l < \theta < \theta_u. \\ -\infty, & \text{otherwise.} \end{cases} \quad (12)$$

¹ In practice it is suitable to work with natural logarithm of the probability distributions (see, e.g., Hogg & Foreman-Mackey (2018))

The luminosity model, $f(\theta)$, we employed is given in Equation (8). We solved the coupled equations, (1) and (2), described in Section 2.1 using `scipy.integrate.odeint` to find $\Omega(t)$ and $\alpha(t)$ and calculated the light curve with Equation (8). In all calculations we fixed the moment of inertia as $I = 10^{45}$ g cm².

In order to calculate the posterior probability distributions of our parameter sets, i.e., $\{P_0, \sin \alpha_0, \mu_0\}$ and $\{P_0, \sin \alpha_0, \mu_0, \mu_\infty, t_m\}$, we used an affine-invariant Markov Chain Monte-Carlo Ensemble sampler, `emcee` (Foreman-Mackey et al. 2013, 2018). We used 500 walkers for each parameter. In the first run of the `emcee` we used 50,000 steps for burn-in phase. In the main phase we adjusted the number of steps according to the integrated autocorrelation time (τ_f) (Goodman & Weare 2010; Foreman-Mackey et al. 2013) which is calculated using `acor` (Foreman-Mackey 2012) package. At every hundred steps we calculated τ_f and its difference from the previous step. When the step number is smaller than $100\tau_f$ and the differences in new and old τ_f value is smaller than 0.01, we assumed that the chain has converged². In order to be more conservative we continued sampling until either the step number is reached up to five hundred times the maximum τ_f or 100,000 steps. Then we “thinned” the sample by the half of the mean τ_f . In the second run of the `emcee` we initialized the chains around a small Gaussian ball of most probable values of the parameters determined in the first run of the `emcee`. The parameter values and their uncertainties are obtained from the median and standard deviation of the posterior probability distributions. Finally, we calculated the evolution of the braking index from Equation (3) and Equation (5) for constant and changing magnetic dipole moment cases, respectively. The triangle plots are plotted with the `getdist` (Lewis et al. 2018) package.

2.3. GRB sample

GRBs display a bimodal distribution of duration (Kouveliotou et al. 1993): the short- ($t < 2$ s) and long-duration bursts ($t \gtrsim 2$ s). Furthermore, the detection of several GRBs with durations exceeding thousands of seconds brought out the possibility of a third class of GRBs named as ultra-long GRBs (Levan et al. 2014) (ULGRBs). Short GRBs have long been considered, on theoretical grounds, to arise from the merger of two neutron stars (Blinnikov et al. 1984; Paczynski 1986; Eichler et al. 1989), an idea which was spectacularly confirmed by the detection of gravitational waves (Abbott et al. 2017a) released during inspiral of two neutron stars associated with GRB 170817 (Abbott et al. 2017b). The merger of binary neutron stars may result with the formation of a rapidly rotating ($P \sim 1$ ms) magnetar (Duncan & Thompson 1992) which is centrifugally supported and may collapse to a black hole upon slow-down. The origin of the long-duration GRBs are understood as the deaths of massive stars in core-collapse supernovae of Type 1c (Woosley 1993). Some long and ultra-long duration GRBs, nevertheless, are also suggested to be associated with magnetars (see, e.g. Gompertz & Fruchter (2017)). Therefore, we do not use the prompt emission duration as a selection criteria for candidate searches since both types could host magnetars.

We obtained GRB light curves from the Swift *XRT* GRB light curve repository³ (Evans et al. 2007, 2009). Exploring all the available GRBs we especially selected the ones which contain plateau phase since those are the most probable candidates for hosting a magnetar as the central engine. We then computed the luminosity values from flux light curves in the Swift *XRT* energy range (0.3 – 10 keV) using

$$L = 4\pi d_L^2(z) F_X k(z) \quad (13)$$

Here, $d_L(z)$ is the luminosity distance which depends on the redshift of the source. F_X is the unabsorbed flux values. We used Swift *XRT* data in photon counting (PC) mode and also included the data from windowed timing (WT) mode if available. k is the cosmological k -correction due to cosmological expansion (Bloom et al. 2001).

$$k(z) = (1+z)^{(\Gamma-2)} \quad (14)$$

Here Γ is the photon index of the power law. We obtained the photon index values from Swift *XRT* GRB lightcurve repository.

We calculated the luminosity distance using a flat Λ CDM cosmological model with cosmological parameters $H_0 = 71$ km s⁻¹ Mpc⁻¹ and $\Omega_M = 0.27$ with `astropy.cosmology` subpackage (Price-Whelan et al. 2018; Astropy Collaboration et al. 2013). We obtained most of the redshift values of the sources from the same GRB light curve repository. For the sources which there is no redshift information in that repository, we used published values from literature. We list these values and their references in Table 2. Due to the limited energy that can be extracted from a

² <https://emcee.readthedocs.io/en/latest/tutorials/monitor/>

³ http://www.swift.ac.uk/xrt_curves/

magnetar, only a subset of the GRBs can be modelled with the magnetar central engine assumption. Here we present the strongest candidates for which the magnetar central engine would be favoured due to the presence of a plateau. We note that although we did not use the duration of GRBs as a selection criteria, we find that all strong candidates listed in Table 2 belong to long-GRB class (Barbier et al. 2006; Stamatikos et al. 2007; Parsons et al. 2007; Barthelmy et al. 2007; Guidorzi et al. 2007; Palmer et al. 2007; Cummings et al. 2014; D’Ai et al. 2016; Palmer et al. 2016; Markwardt et al. 2009).

3. RESULTS AND DISCUSSION

We modelled the X-ray afterglow light curves of seven long GRBs with magnetic dipole radiation model described in § 2.1. Four GRBs in our sample (see Table 2), GRBs 060510A, 070420, 070521 and 140629A, are best modelled with a constant magnetic dipole moment (see Table 3). We present the evolution of luminosity, period, inclination angle and braking index of these GRBs in Figures 1, 2, 3 and 4 (left panels). In three cases, GRBs 070508, 091018 and 161219B, the model with constant magnetic dipole moment resulted in reduced chi-squared values greater than ~ 3 . Consequently, for these GRBs we allowed the evolution of the magnetic dipole moment according to Equation (4). We find that for these GRBs magnetic dipole moments of the magnetars decrease rapidly. The putative nascent magnetar parameters including the evolutionary time-scale of the magnetic dipole moment and its relaxed value for the three GRBs are listed in Table 4 and evolution of the parameters is presented in Figures 5, 6 and 7 (left panels). 1D and 2D posterior probability distributions of the parameters for all GRBs are shown on the right panel of each figure.

The drop in the magnetic dipole moment, $\mu = \frac{1}{2}BR^3$, might either be due to a decaying magnetic field, B , or the radius of the star, R , settling. However, the time-scale for the settling of the radius of a proto-neutron star is ~ 10 s (Burrows & Lattimer 1986) which is much shorter than the time-scale for the evolution of the magnetic moment inferred in this work, 0.02 – 0.3 day. It is then unlikely that the change in the magnetic moment is due to the change in the radius of the star. The time-scale for the change in the magnetic dipole moment inferred from the fits is much shorter than the secular magnetic field decay time-scale in the magnetar model (Colpi et al. 2000) $\sim 10^3$ yr. What we “observe” here could be the tail of the strong $B \sim 10^{16}$ G magnetic field associated with the prompt emission (Beniamini et al. 2017).

It is interesting to see that for the 7 GRBs we analysed the inclination angles of nascent magnetars at the start of the plateau phase are found to have values distributed in the narrow range of $\sim 30^\circ - 45^\circ$. As a result of the alignment between the rotation and the magnetic axis, the spin-down luminosity, L declines less rapidly than $L \propto t^{-2}$ resulting from pure spin-down. One requires magnetars with higher magnetic dipole moments to address a certain light curve. Note that all the P_0 , μ_0 curves in Fig. 8 remain below the canonical $P_0 = 1$ ms, $\mu_0 = 1 \times 10^{33}$ G cm³ point. It is remarkable that the light curves could be modelled by assuming slower rotating ($P_0 \sim 10$ ms) magnetars with very strong magnetic dipole moments ($\mu_0 \sim 10^{34}$ G cm³) depending on the value of η .

In the model employed here the inclination angle approaches to small values as $\alpha \propto (t/t_0)^{-1/2}$ in a spin-down time-scale (Philippov et al. 2014). Drastic changes observed in the inclination angle and magnetic dipole moment, as well as the spin period during the extended emission stage of nascent magnetars may be caused simply because the star, initially, is in an extreme stage displaying transient behaviour. This is demonstrated by the obvious evolution of the inclination angle, as prominent as the evolution in the spin period. The same alignment torque would also lead to the formation of very young neutron stars with aligned conventional ($B \sim 10^{12}$ G) magnetic fields though in a longer time scale. Such objects, however, can not show up as a rotationally powered pulsars. This may explain the lack of detection of a rotationally powered pulsar in SN 87A (Alp et al. 2018) and the central compact object in Cas A (Chakrabarty et al. 2001). This picture, in order to address the existence of many young rotationally powered pulsars, such as Crab, requires that the inclination angle that is reduced during the first years following birth should increase in the longer term. There is indeed evidence that inclination angle of the Crab pulsar has been increasing at a rate $0.62^\circ \pm 0.03^\circ$ per century (Lyne et al. 2013). The cause of this counter-alignment is yet to be clarified.

This work made use of data supplied by the UK Swift Science Data Centre at the University of Leicester (http://www.swift.ac.uk/xrt_curves/). SSM acknowledges post-doctoral research support from İstanbul Technical University. SSM and KYE acknowledges support from TÜBİTAK, The Scientific and Technological Research Council of Turkey, with the project number 118F028.

Facilities: Swift (*XRT*)

Software: `Astropy` (Price-Whelan et al. 2018; Astropy Collaboration et al. 2013), `Matplotlib` (Hunter 2007), `SciPy` (Jones et al. 2001), `emcee` (Foreman-Mackey et al. 2013, 2018), `getdist` (Lewis et al. 2018), `acor` (Foreman-Mackey 2012), `gnuplot` (Williams et al. 2013)

REFERENCES

- Abbott, B. P., Abbott, R., Abbott, T. D., et al. 2017a, Physical Review Letters, 119, 161101, doi: [10.1103/PhysRevLett.119.161101](https://doi.org/10.1103/PhysRevLett.119.161101)
- . 2017b, ApJL, 848, L12, doi: [10.3847/2041-8213/aa91c9](https://doi.org/10.3847/2041-8213/aa91c9)
- Akiyama, S., Wheeler, J. C., Meier, D. L., & Lichtenstadt, I. 2003, ApJ, 584, 954, doi: [10.1086/344135](https://doi.org/10.1086/344135)
- Alp, D., Larsson, J., Fransson, C., et al. 2018, ApJ, 864, 174, doi: [10.3847/1538-4357/aad739](https://doi.org/10.3847/1538-4357/aad739)
- Antonopoulou, D., Weltevrede, P., Espinoza, C. M., et al. 2015, MNRAS, 447, 3924, doi: [10.1093/mnras/stu2710](https://doi.org/10.1093/mnras/stu2710)
- Archibald, R. F., Kaspi, V. M., Beardmore, A. P., Gehrels, N., & Kennea, J. A. 2015, ApJ, 810, 67, doi: [10.1088/0004-637X/810/1/67](https://doi.org/10.1088/0004-637X/810/1/67)
- Archibald, R. F., Gotthelf, E. V., Ferdman, R. D., et al. 2016, ApJL, 819, L16, doi: [10.3847/2041-8205/819/1/L16](https://doi.org/10.3847/2041-8205/819/1/L16)
- Arzamasskiy, L., Philippov, A., & Tchekhovskoy, A. 2015, MNRAS, 453, 3540, doi: [10.1093/mnras/stv1818](https://doi.org/10.1093/mnras/stv1818)
- Astropy Collaboration, Robitaille, T. P., Tollerud, E. J., et al. 2013, A&A, 558, A33, doi: [10.1051/0004-6361/201322068](https://doi.org/10.1051/0004-6361/201322068)
- Barbier, L., Barthelmy, S., Cummings, J., et al. 2006, GRB Coordinates Network, 5108
- Barthelmy, S. D., Barbier, L., Cummings, J., et al. 2007, GRB Coordinates Network, 6390
- Beniamini, P., Giannios, D., & Metzger, B. D. 2017, MNRAS, 472, 3058, doi: [10.1093/mnras/stx2095](https://doi.org/10.1093/mnras/stx2095)
- Blinnikov, S. I., Novikov, I. D., Perevodchikova, T. V., & Polnarev, A. G. 1984, Soviet Astronomy Letters, 10, 177, <https://arxiv.org/abs/1808.05287>
- Bloom, J. S., Frail, D. A., & Sari, R. 2001, AJ, 121, 2879, doi: [10.1086/321093](https://doi.org/10.1086/321093)
- Bucciantini, N., Quataert, E., Arons, J., Metzger, B. D., & Thompson, T. A. 2008, MNRAS, 383, L25, doi: [10.1111/j.1745-3933.2007.00403.x](https://doi.org/10.1111/j.1745-3933.2007.00403.x)
- Burrows, A., & Lattimer, J. M. 1986, ApJ, 307, 178, doi: [10.1086/164405](https://doi.org/10.1086/164405)
- Chakrabarty, D., Pivovaroff, M. J., Hernquist, L. E., Heyl, J. S., & Narayan, R. 2001, ApJ, 548, 800, doi: [10.1086/318994](https://doi.org/10.1086/318994)
- Cheng, Q., & Yu, Y.-W. 2014, ApJL, 786, L13, doi: [10.1088/2041-8205/786/2/L13](https://doi.org/10.1088/2041-8205/786/2/L13)
- Colpi, M., Geppert, U., & Page, D. 2000, ApJL, 529, L29, doi: [10.1086/312448](https://doi.org/10.1086/312448)
- Cummings, J. R., Barthelmy, S. D., Baumgartner, W. H., et al. 2014, GRB Coordinates Network, Circular Service, No. 16481, #1 (2014), 16481
- D’Ai, A., Kennea, J. A., Krimm, H. A., et al. 2016, GRB Coordinates Network, Circular Service, No. 20296, #1 (2016), 20296
- Dai, Z. G., & Lu, T. 1998a, A&A, 333, L87
- . 1998b, Physical Review Letters, 81, 4301, doi: [10.1103/PhysRevLett.81.4301](https://doi.org/10.1103/PhysRevLett.81.4301)
- Dall’Osso, S., Stratta, G., Guetta, D., et al. 2011, A&A, 526, A121, doi: [10.1051/0004-6361/201014168](https://doi.org/10.1051/0004-6361/201014168)
- Duncan, R. C., & Thompson, C. 1992, ApJL, 392, L9, doi: [10.1086/186413](https://doi.org/10.1086/186413)
- Eichler, D., Livio, M., Piran, T., & Schramm, D. N. 1989, Nature, 340, 126, doi: [10.1038/340126a0](https://doi.org/10.1038/340126a0)
- Ekşi, K. Y. 2017, MNRAS, 469, 1974, doi: [10.1093/mnras/stx1035](https://doi.org/10.1093/mnras/stx1035)
- Ekşi, K. Y., Andaç, I. C., Çıkıntıoğlu, S., et al. 2016, ApJ, 823, 34, doi: [10.3847/0004-637X/823/1/34](https://doi.org/10.3847/0004-637X/823/1/34)
- Espinoza, C. M., Lyne, A. G., Kramer, M., Manchester, R. N., & Kaspi, V. M. 2011, ApJL, 741, L13, doi: [10.1088/2041-8205/741/1/L13](https://doi.org/10.1088/2041-8205/741/1/L13)
- Evans, P. A., Beardmore, A. P., Page, K. L., et al. 2007, A&A, 469, 379, doi: [10.1051/0004-6361:20077530](https://doi.org/10.1051/0004-6361:20077530)
- . 2009, MNRAS, 397, 1177, doi: [10.1111/j.1365-2966.2009.14913.x](https://doi.org/10.1111/j.1365-2966.2009.14913.x)
- Fan, Y.-Z., & Xu, D. 2006, MNRAS, 372, L19, doi: [10.1111/j.1745-3933.2006.00217.x](https://doi.org/10.1111/j.1745-3933.2006.00217.x)
- Fan, Y.-Z., Yu, Y.-W., Xu, D., et al. 2013, ApJL, 779, L25, doi: [10.1088/2041-8205/779/2/L25](https://doi.org/10.1088/2041-8205/779/2/L25)
- Ferdman, R. D., Archibald, R. F., & Kaspi, V. M. 2015, ApJ, 812, 95, doi: [10.1088/0004-637X/812/2/95](https://doi.org/10.1088/0004-637X/812/2/95)
- Foreman-Mackey, D. 2012, acor, GitHub. <https://github.com/dfm/acor>
- Foreman-Mackey, D., Hogg, D. W., Lang, D., & Goodman, J. 2013, PASP, 125, 306, doi: [10.1086/670067](https://doi.org/10.1086/670067)
- Foreman-Mackey, D., Farr, W. M., Tollerud, E., et al. 2018, emcee, v3.0rc2, Zenodo, doi: [10.5281/zenodo.1436565](https://doi.org/10.5281/zenodo.1436565). <http://doi.org/10.5281/zenodo.1436565>
- Gold, T. 1968, Nature, 218, 731, doi: [10.1038/218731a0](https://doi.org/10.1038/218731a0)
- Goldreich, P. 1970, ApJL, 160, L11, doi: [10.1086/180513](https://doi.org/10.1086/180513)
- Goldreich, P., & Julian, W. H. 1969, ApJ, 157, 869, doi: [10.1086/150119](https://doi.org/10.1086/150119)

- Gompertz, B., & Fruchter, A. 2017, ApJ, 839, 49, doi: [10.3847/1538-4357/aa6629](https://doi.org/10.3847/1538-4357/aa6629)
- Gompertz, B. P., O'Brien, P. T., Wynn, G. A., & Rowlinson, A. 2013, MNRAS, 431, 1745, doi: [10.1093/mnras/stt293](https://doi.org/10.1093/mnras/stt293)
- Goodman, J., & Weare, J. 2010, Communications in Applied Mathematics and Computational Science, Vol. 5, No. 1, p. 65-80, 2010, 5, 65, doi: [10.2140/camcos.2010.5.65](https://doi.org/10.2140/camcos.2010.5.65)
- Guidorzi, C., Barthelmy, S. D., Evans, P. A., et al. 2007, GRB Coordinates Network, 6431
- Hogg, D. W., & Foreman-Mackey, D. 2018, ApJS, 236, 11, doi: [10.3847/1538-4365/aab76e](https://doi.org/10.3847/1538-4365/aab76e)
- Hunter, J. D. 2007, Computing In Science & Engineering, 9, 90, doi: [10.1109/MCSE.2007.55](https://doi.org/10.1109/MCSE.2007.55)
- Jones, E., Oliphant, T., Peterson, P., et al. 2001, SciPy: Open source scientific tools for Python.
<http://www.scipy.org/>
- Kluźniak, W., & Ruderman, M. 1998, ApJL, 505, L113, doi: [10.1086/311622](https://doi.org/10.1086/311622)
- Knust, F., Greiner, J., van Eerten, H. J., et al. 2017, A&A, 607, A84, doi: [10.1051/0004-6361/201730578](https://doi.org/10.1051/0004-6361/201730578)
- Kouveliotou, C., Meegan, C. A., Fishman, G. J., et al. 1993, ApJL, 413, L101, doi: [10.1086/186969](https://doi.org/10.1086/186969)
- Lander, S. K., & Jones, D. I. 2018, MNRAS, 481, 4169, doi: [10.1093/mnras/sty2553](https://doi.org/10.1093/mnras/sty2553)
- Lasky, P. D., Leris, C., Rowlinson, A., & Glampedakis, K. 2017, ApJL, 843, L1, doi: [10.3847/2041-8213/aa79a7](https://doi.org/10.3847/2041-8213/aa79a7)
- Levan, A. J., Tanvir, N. R., Starling, R. L. C., et al. 2014, ApJ, 781, 13, doi: [10.1088/0004-637X/781/1/13](https://doi.org/10.1088/0004-637X/781/1/13)
- Lewis, A., Handley, W., Xu, Y., Torrado, J., & Higson, E. 2018, GetDist, 0.3.0, Zenodo, doi: [10.5281/zenodo.1415428](https://doi.org/10.5281/zenodo.1415428).
<http://doi.org/10.5281/zenodo.1415428>
- Li, L., Wu, X.-F., Lei, W.-H., et al. 2018, ApJS, 236, 26, doi: [10.3847/1538-4365/aabaf3](https://doi.org/10.3847/1538-4365/aabaf3)
- Livingstone, M. A., & Kaspi, V. M. 2011, ApJ, 742, 31, doi: [10.1088/0004-637X/742/1/31](https://doi.org/10.1088/0004-637X/742/1/31)
- Livingstone, M. A., Kaspi, V. M., Gavriil, F. P., et al. 2007, Ap&SS, 308, 317, doi: [10.1007/s10509-007-9320-3](https://doi.org/10.1007/s10509-007-9320-3)
- Lü, H.-J., Lan, L., & Liang, E.-W. 2019, ApJ, 871, 54, doi: [10.3847/1538-4357/aaf71d](https://doi.org/10.3847/1538-4357/aaf71d)
- Lü, H.-J., & Zhang, B. 2014, ApJ, 785, 74, doi: [10.1088/0004-637X/785/1/74](https://doi.org/10.1088/0004-637X/785/1/74)
- Lü, H.-J., Zhang, H.-M., Zhong, S.-Q., et al. 2017, ApJ, 835, 181, doi: [10.3847/1538-4357/835/2/181](https://doi.org/10.3847/1538-4357/835/2/181)
- Lyne, A., Graham-Smith, F., Weltevreden, P., et al. 2013, Science, 342, 598, doi: [10.1126/science.1243254](https://doi.org/10.1126/science.1243254)
- Lyne, A. G., Pritchard, R. S., & Graham-Smith, F. 1993, MNRAS, 265, 1003
- Lyne, A. G., Pritchard, R. S., Graham-Smith, F., & Camilo, F. 1996, Nature, 381, 497, doi: [10.1038/381497a0](https://doi.org/10.1038/381497a0)
- Markwardt, C. B., Barthelmy, S. D., Baumgartner, W. H., et al. 2009, GRB Coordinates Network, Circular Service, No. 1040, #1 (2009), 10040
- Metzger, B. D., Giannios, D., Thompson, T. A., Bucciantini, N., & Quataert, E. 2011, MNRAS, 413, 2031, doi: [10.1111/j.1365-2966.2011.18280.x](https://doi.org/10.1111/j.1365-2966.2011.18280.x)
- Oates, S. R., Page, M. J., De Pasquale, M., et al. 2012, MNRAS, 426, L86, doi: [10.1111/j.1745-3933.2012.01331.x](https://doi.org/10.1111/j.1745-3933.2012.01331.x)
- Pacini, F. 1968, Nature, 219, 145, doi: [10.1038/219145a0](https://doi.org/10.1038/219145a0)
- Paczynski, B. 1986, ApJL, 308, L43, doi: [10.1086/184740](https://doi.org/10.1086/184740)
- Palmer, D., Barbier, L., Barthelmy, S. D., et al. 2007, GRB Coordinates Network, 6440
- Palmer, D. M., Barthelmy, S. D., Cummings, J. R., et al. 2016, GRB Coordinates Network, Circular Service, No. 20308, #1 (2016), 20308
- Parsons, A., Barbier, L., Barthelmy, S. D., et al. 2007, GRB Coordinates Network, 6342
- Philippov, A., Tchekhovskoy, A., & Li, J. G. 2014, MNRAS, 441, 1879, doi: [10.1093/mnras/stu591](https://doi.org/10.1093/mnras/stu591)
- Price-Whelan, A. M., Sipőcz, B. M., Günther, H. M., et al. 2018, AJ, 156, 123, doi: [10.3847/1538-3881/aabc4f](https://doi.org/10.3847/1538-3881/aabc4f)
- Rea, N., Gullón, M., Pons, J. A., et al. 2015, ApJ, 813, 92, doi: [10.1088/0004-637X/813/2/92](https://doi.org/10.1088/0004-637X/813/2/92)
- Rowlinson, A., Gompertz, B. P., Dainotti, M., et al. 2014, MNRAS, 443, 1779, doi: [10.1093/mnras/stu1277](https://doi.org/10.1093/mnras/stu1277)
- Rowlinson, A., O'Brien, P. T., Metzger, B. D., Tanvir, N. R., & Levan, A. J. 2013, MNRAS, 430, 1061, doi: [10.1093/mnras/sts683](https://doi.org/10.1093/mnras/sts683)
- Rowlinson, A., O'Brien, P. T., Tanvir, N. R., et al. 2010, MNRAS, 409, 531, doi: [10.1111/j.1365-2966.2010.17354.x](https://doi.org/10.1111/j.1365-2966.2010.17354.x)
- Roy, J., Gupta, Y., & Lewandowski, W. 2012, MNRAS, 424, 2213, doi: [10.1111/j.1365-2966.2012.21380.x](https://doi.org/10.1111/j.1365-2966.2012.21380.x)
- Sivia, D. S., & Skilling, J. 2006, Data Analysis: A Bayesian Tutorial (Oxford University Press)
- Spitkovsky, A. 2006, ApJL, 648, L51, doi: [10.1086/507518](https://doi.org/10.1086/507518)
- Stamatikos, M., Burrows, D. N., Cusumano, G., et al. 2007, GRB Coordinates Network, 6330
- Stratta, G., Dainotti, M. G., Dall'Osso, S., Hernandez, X., & De Cesare, G. 2018, ApJ, 869, 155, doi: [10.3847/1538-4357/aadd8f](https://doi.org/10.3847/1538-4357/aadd8f)
- Troja, E., Cusumano, G., O'Brien, P. T., et al. 2007, ApJ, 665, 599, doi: [10.1086/519450](https://doi.org/10.1086/519450)
- Usov, V. V. 1992, Nature, 357, 472, doi: [10.1038/357472a0](https://doi.org/10.1038/357472a0)
- Williams, T., Kelley, C., & many others. 2013, Gnuplot 4.6: an interactive plotting program,
<http://gnuplot.sourceforge.net/>
- Woosley, S. E. 1993, ApJ, 405, 273, doi: [10.1086/172359](https://doi.org/10.1086/172359)

- Xiao, L., & Schaefer, B. E. 2011, ApJ, 731, 103,
doi: [10.1088/0004-637X/731/2/103](https://doi.org/10.1088/0004-637X/731/2/103)
- Zhang, B., & Mészáros, P. 2001, ApJL, 552, L35,
doi: [10.1086/320255](https://doi.org/10.1086/320255)
- Xu, M., & Huang, Y.-F. 2015, Research in Astronomy and
Astrophysics, 15, 986, doi: [10.1088/1674-4527/15/7/006](https://doi.org/10.1088/1674-4527/15/7/006)

Table 1. Parameter Boundaries for Uniform Prior Distributions.

Parameters	Lower Limit	Upper Limit
P_0 (ms)	0.70	10^2
$\sin \alpha_0$	10^{-3}	0.99
μ_0 (10^{33} G cm 3)	10^{-3}	10
μ_∞ (10^{33} G cm 3)	10^{-3}	10
t_m (day)	10^{-4}	10^2

Table 2. GRB Sample and Its Parameters

GRB	Redshift ^a	Photon Index
	(z)	Γ
060510A	1.2 ^b	1.81 ± 0.08
070420	0.66 ^c	1.778 ± 0.095
070521	2.0865	1.89 ± 0.13
140629A	2.275	1.96 ± 0.11
070508	0.82	1.79 ± 0.135
091018	0.971	2.0 ± 0.115
161219B	0.1475	1.83 ± 0.06

^aRedshift and photon index values are taken from the Swift *XRT* GRB lightcurve repository (Evans et al. 2007, 2009) unless otherwise stated.

^bXiao & Schaefer (2011)

^cOates et al. (2012)

Table 3. Estimated Values of the Putative Nascent Magnetar Parameters for Constant Magnetic Dipole Moment Case.

GRB	P_0 (ms)	$\sin \alpha_0$	μ_0 (10^{33} G cm 3)	χ^2/dof
060510A	1.057 ± 0.010	0.675 ± 0.069	0.232 ± 0.009	163.17/159
070420	3.916 ± 0.040	0.623 ± 0.092	1.012 ± 0.049	178.87/142
070521	1.357 ± 0.024	0.508 ± 0.201	0.699 ± 0.055	81.62/82
140629A	1.951 ± 0.027	0.586 ± 0.172	1.149 ± 0.085	66.96/89

Table 4. Estimated Values of the Putative Nascent Magnetar Parameters for Changing Magnetic Dipole Moment Case.

GRB	P_0 (ms)	$\sin \alpha_0$	μ_0 (10^{33} G cm 3)	μ_∞ (10^{33} G cm 3)	t_m (days)	χ^2/dof
070508	2.016 ± 0.016	0.634 ± 0.213	1.258 ± 0.112	0.782 ± 0.065	0.014 ± 0.003	426.58/483
091018	2.922 ± 0.039	0.524 ± 0.236	1.834 ± 0.174	0.683 ± 0.063	0.016 ± 0.002	139.23/134
161219B	7.088 ± 0.055	0.617 ± 0.085	0.508 ± 0.024	0.178 ± 0.009	0.281 ± 0.018	660.70/407

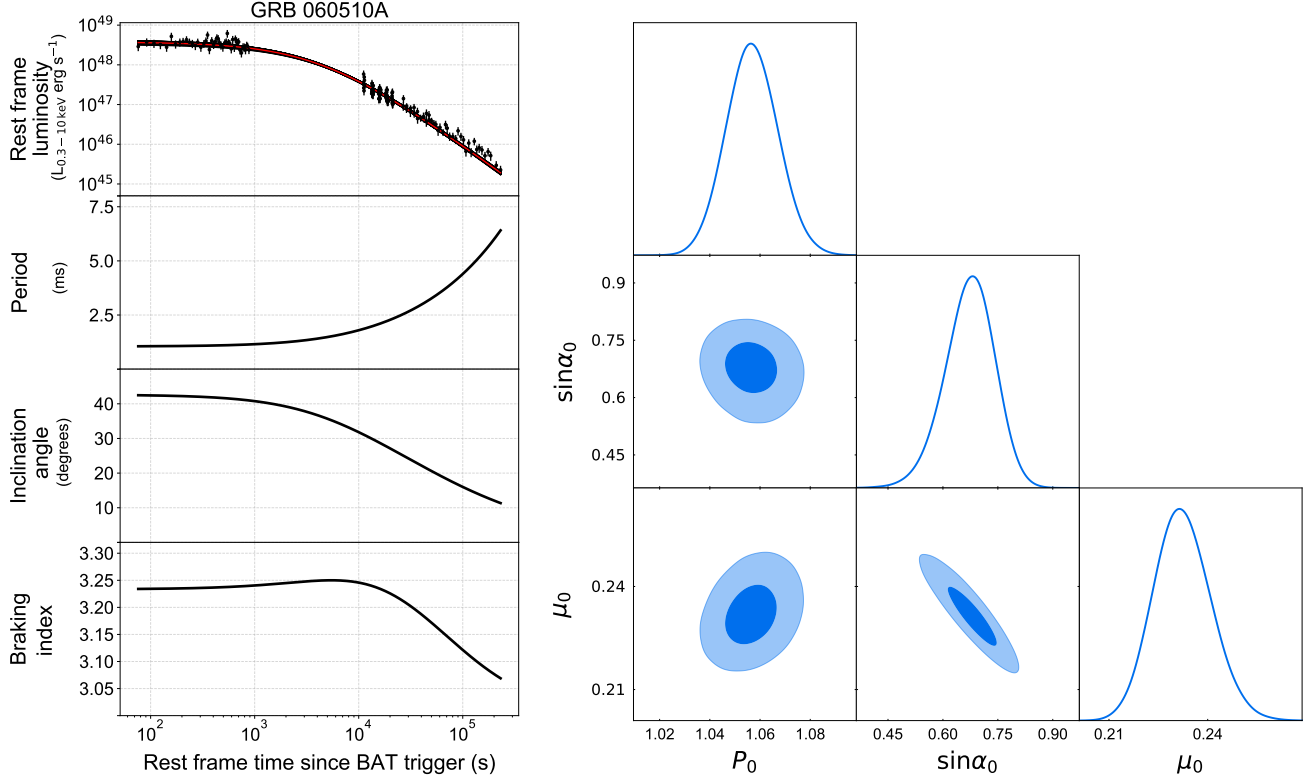


Figure 1. Evolution of putative nascent magnetar parameters and triangle plot for GRB 060510A. Left panel: Luminosity, period, inclination angle and braking index evolution of the putative nascent magnetar in GRB 060510A for the constant magnetic dipole moment case. Solid black lines in the luminosity evolution panel represent 500 models randomly selected from the posterior probability distribution and the red line represents the median value of all samples. Right panel: 1D and 2D posterior probability distributions of the parameters. Contours indicate 1 and 2 sigma levels.

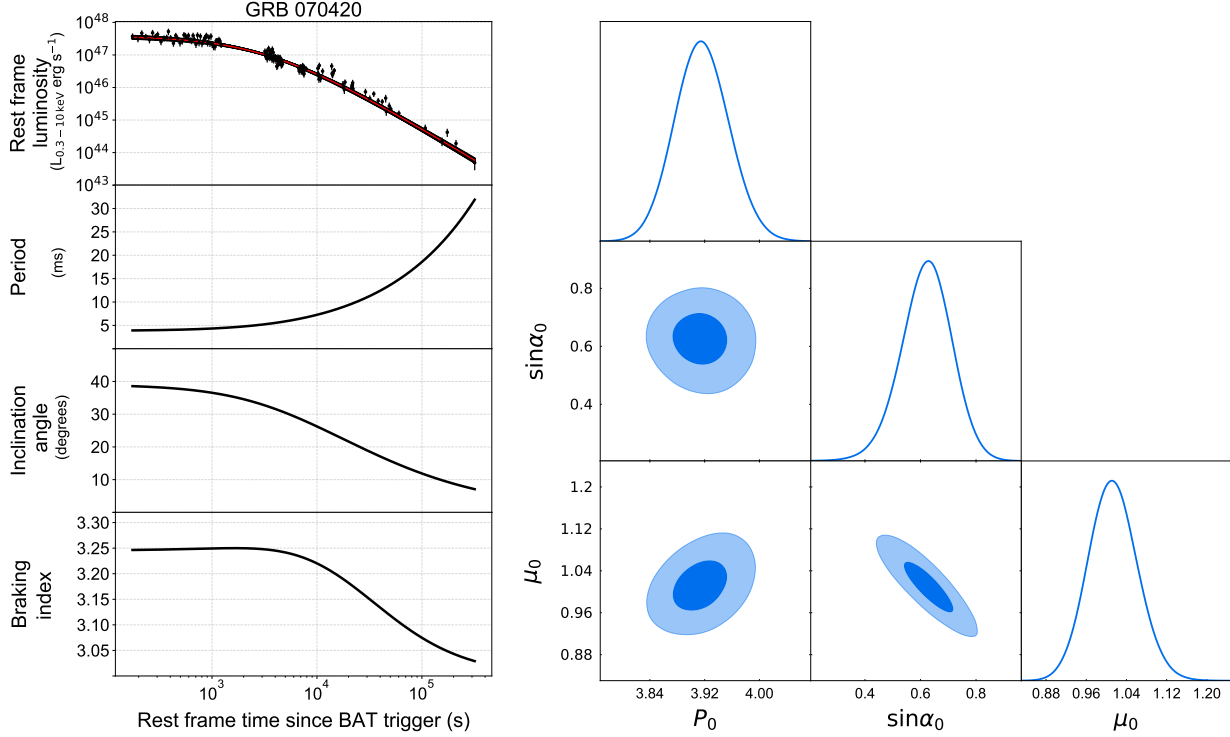


Figure 2. Evolution of putative nascent magnetar parameters and triangle plot for GRB 070420. Same as Figure 1, but for GRB 070420.

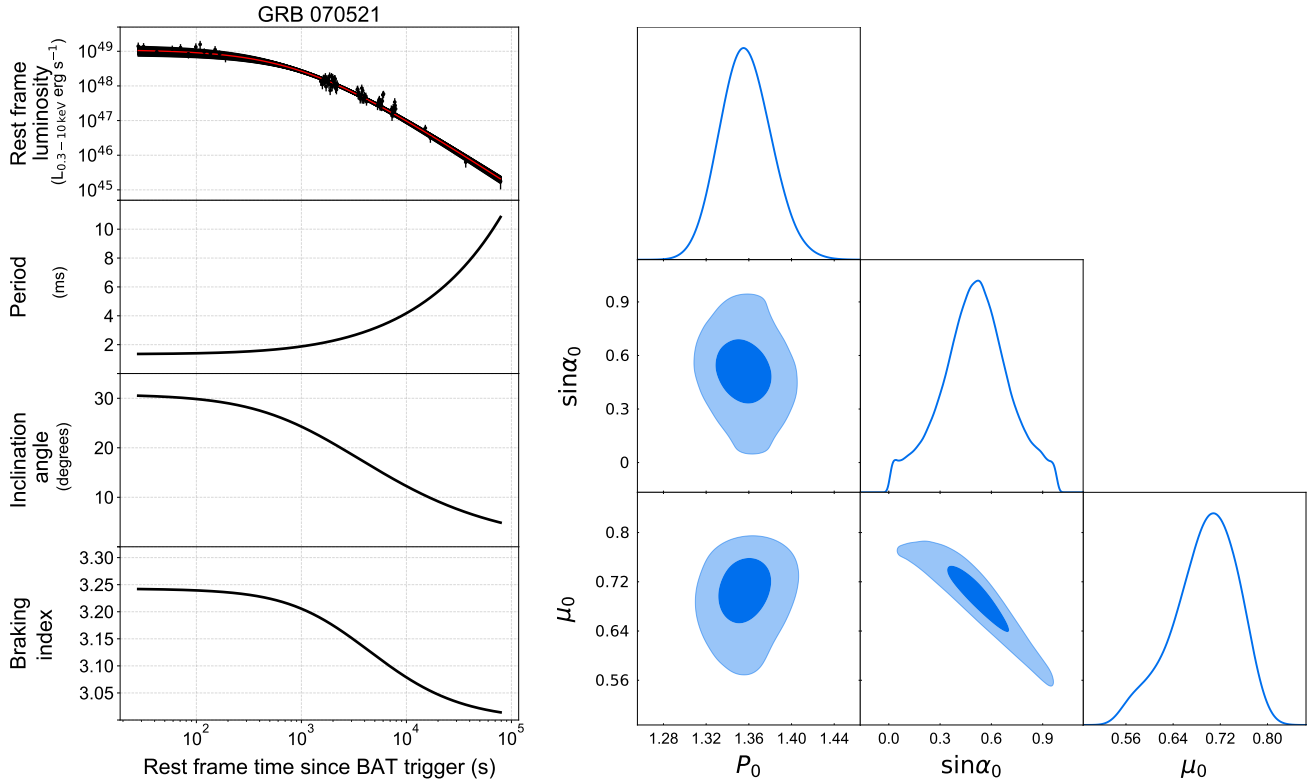


Figure 3. Evolution of putative nascent magnetar parameters and triangle plot for GRB 070521. Same as Figure 1, but for GRB 070521.

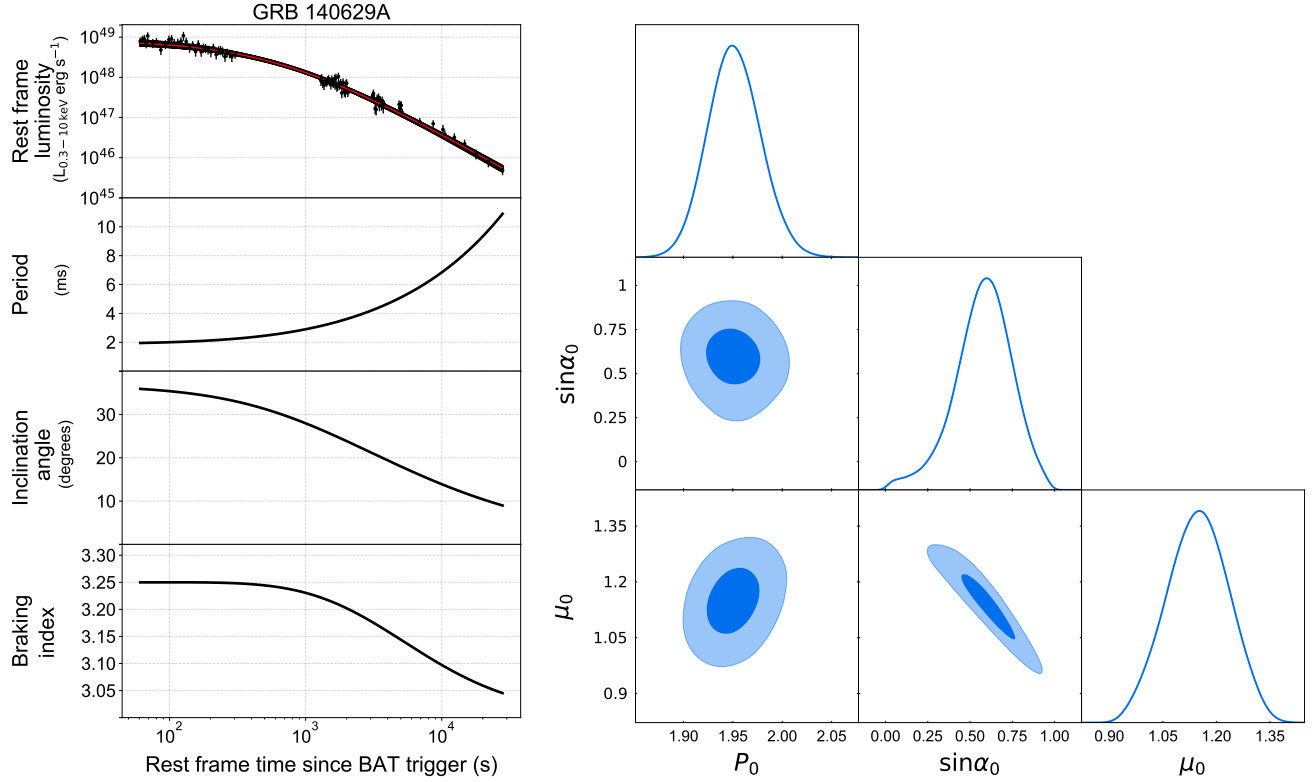


Figure 4. Evolution of putative nascent magnetar parameters and triangle plot for GRB 140629A. Same as Figure 1, but for GRB 140629A.

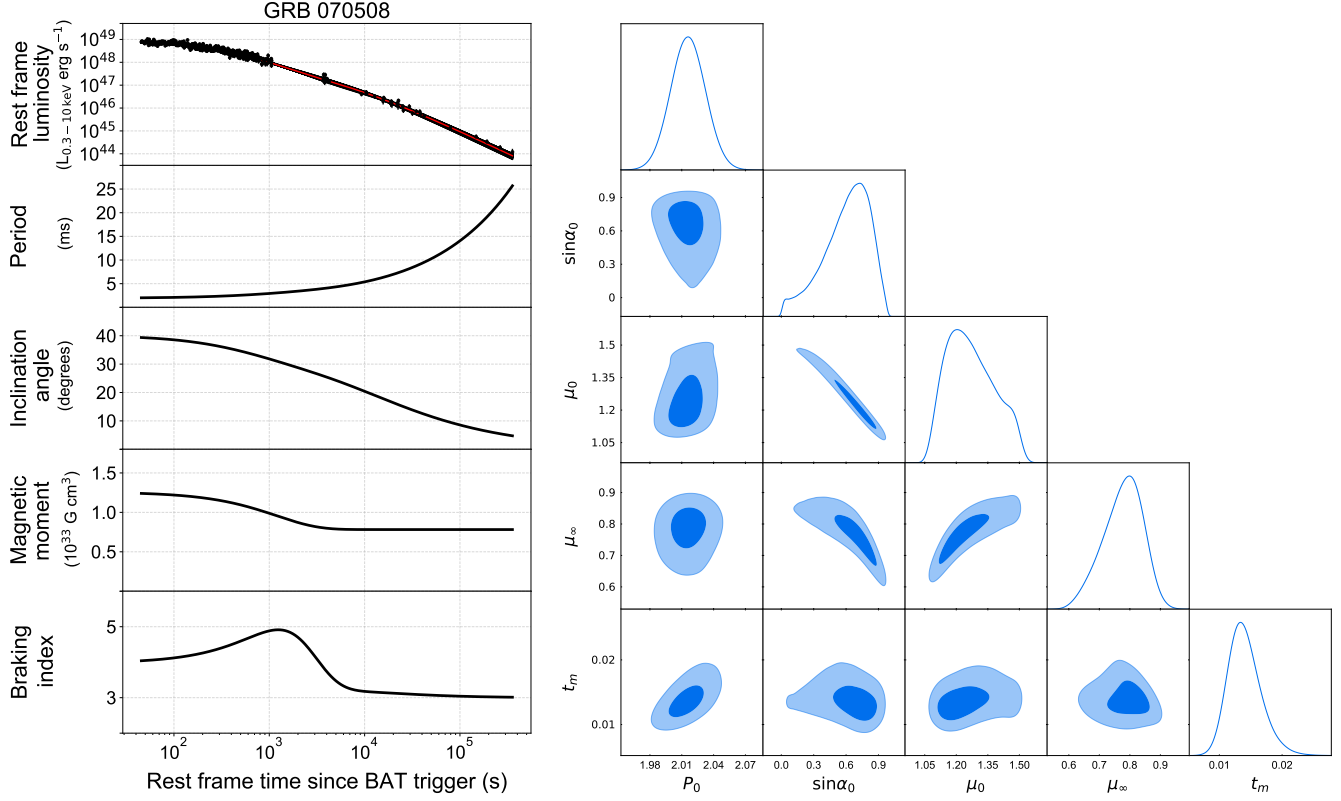


Figure 5. Evolution of putative nascent magnetar parameters and triangle plot for GRB 070508. (a) Luminosity, period, inclination angle, magnetic dipole moment and braking index evolution of the putative nascent magnetar in GRB 070508 for the changing magnetic dipole moment case. Solid black lines in the luminosity evolution panel represent 500 models randomly selected from the posterior probability distribution and the red line represents the median value of all samples. **Right panel:** 1D and 2D posterior probability distributions of the parameters. Contours indicate 1 and 2 sigma levels.

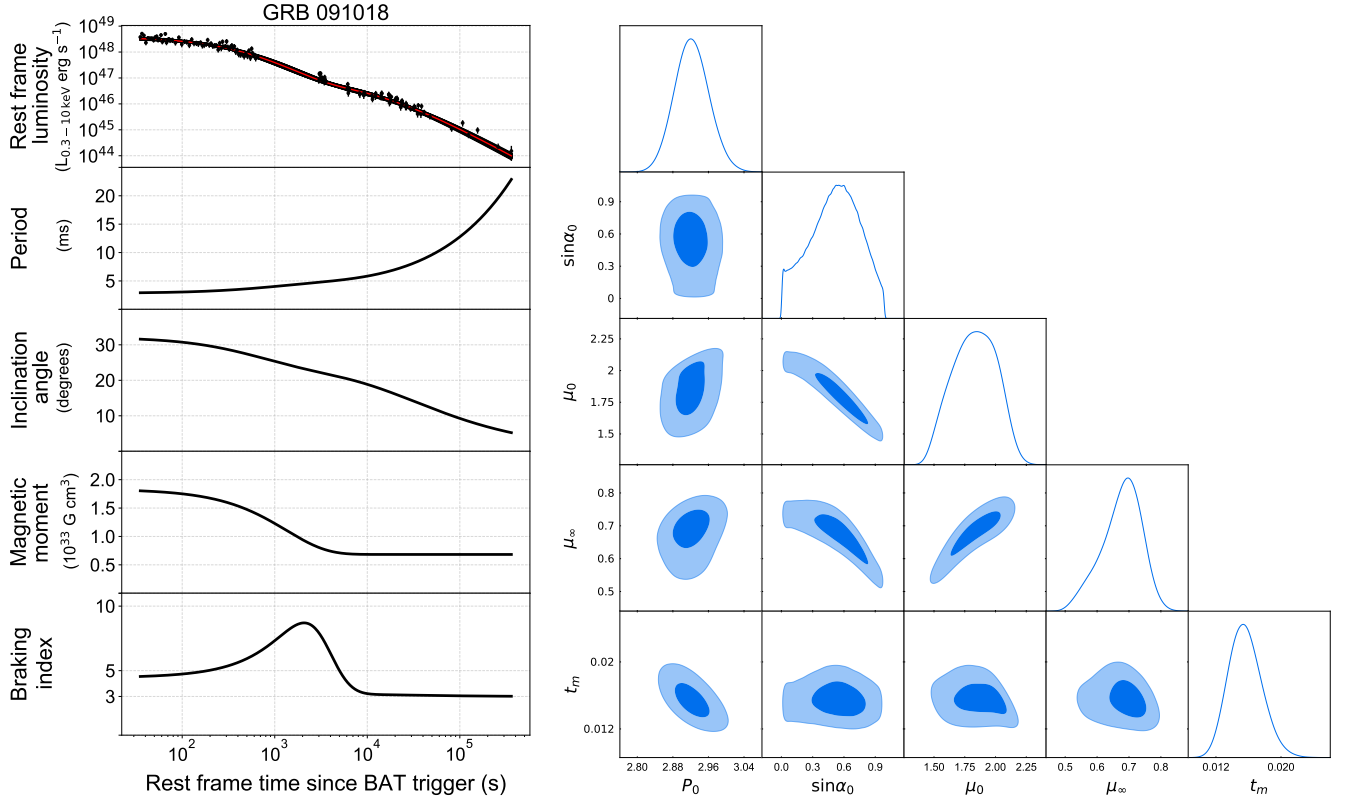


Figure 6. Evolution of putative nascent magnetar parameters and triangle plot for GRB 091018. Same as Figure 5, but for GRB 091018. We note that this source is also investigated by Lü et al. (2019). They find a braking index of 4.12 ± 0.04 for the putative nascent magnetar in the case of constant inclination angle and magnetic dipole moment.

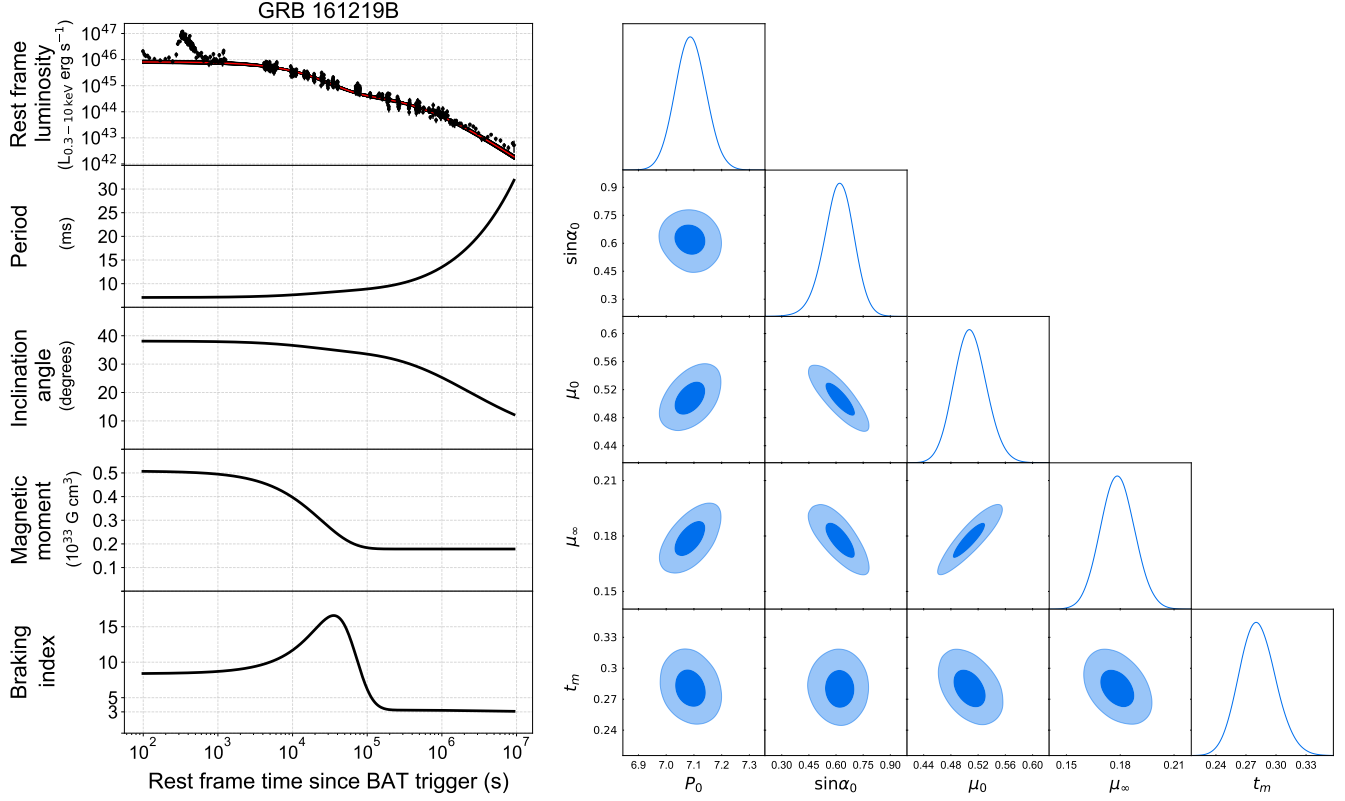


Figure 7. Evolution of putative nascent magnetar parameters and triangle plot for GRB 161219B. Same as Figure 5, but for GRB 161219B. Note that we didn't include the flare in our analysis.

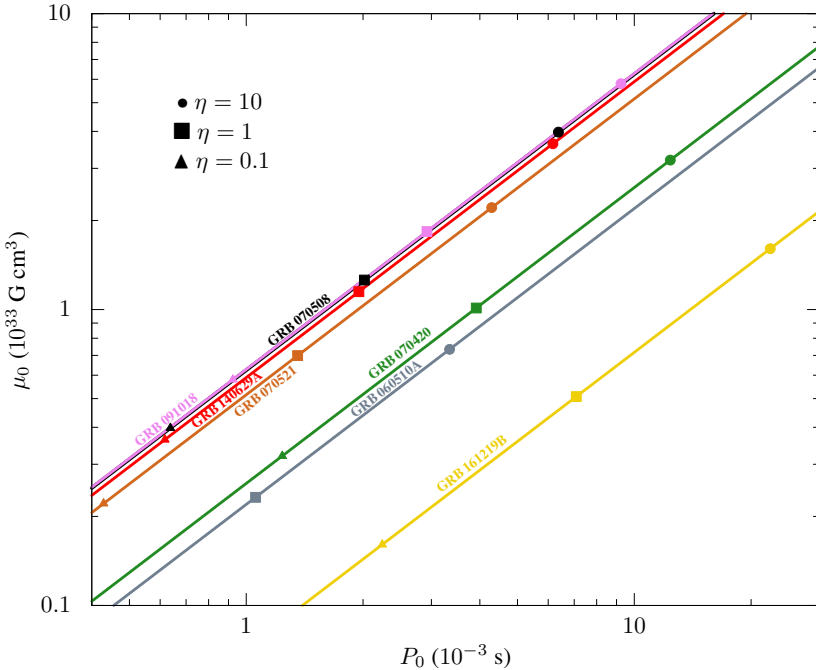


Figure 8. Possible values of P_0 and μ_0 for different values of η .